



---

# Design Parameters for Neckform Modifications and Development

---

NHTSA Cooperative Agreement No.:

*DTNH22-94-Y-07133*

Revised, January 20, 2000

---

Investigators:

Roger W. Nightingale, Ph.D.  
Chris A. Van Ee, B.S.E.  
Barry S. Myers, M.D., Ph.D.

Duke University  
Department of Biomedical Engineering  
Box 90281  
Durham, NC 27709-0281

## Table of Contents

<i>Table of Contents</i> .....	2
<b>Introduction</b> .....	<b>3</b>
<b>Design Parameters for Bending Responses</b> .....	<b>3</b>
<i>Static Flexibility of the Upper Cervical Spine</i> .....	3
<i>Tolerance for Upper Cervical Spine Bending Injury</i> .....	4
<i>Dynamic Flexibility of the Upper Cervical Spine</i> .....	6
<i>Static Flexibility of the Lower Cervical Spine</i> .....	6
<i>Tolerance for Lower Cervical Spine Bending Injury</i> .....	6
<i>Dynamic Flexibility of the Lower Cervical Spine</i> .....	7
<b>Design Parameters for Tensile Responses</b> .....	<b>9</b>
<i>Tensile Stiffness of the Whole Ligamentous Cervical Spine</i> .....	9
<i>Tensile Tolerance Data for Motion Segments</i> .....	10
<i>Tensile Stiffness of Cervical Spine Motion Segments</i> .....	10
<b>The Effects of the Musculature</b> .....	<b>11</b>
<b>Facilities for Neckform Testing</b> .....	<b>12</b>
<i>Bending Design Test</i> :.....	12
<i>Bending Performance Test</i> .....	13
<i>Compression Design Test</i> .....	13
<i>Compression Performance Test</i> .....	13
<i>Tension Testing</i> .....	13
<b>Conclusions</b> .....	<b>13</b>

## Introduction

Data presented in this report is based on preliminary analysis from an ongoing experimental program. The results are based on bending tests from 15 female cadaver specimens, and on tension tests from five male cadaver specimens. As such, the parameters will be refined as the program progresses. This is particularly true of the tension data.

## Design Parameters for Bending Responses

### Static Flexibility of the Upper Cervical Spine

Pure moment testing was performed on 15 Occiput-C2 motion segments from female cadavers. The motion segments were cast into aluminum cups with reinforced polyester resin. Upper cervical specimens (Occiput-C2) were inverted and mounted in the test frame using halo fixation of the head and casting of the C2 vertebra. After being mounted in the test frame, specimens were preconditioned for 30 cycles of flexion and extension. A pneumatic test apparatus was used to apply pure flexion and extension moments in 0.5 N-m increments to a peak of approximately 3.5 N-m. A six-axis load cell was used to measure the loads at the base of the specimen and ensure that the applied bending moment remained pure.

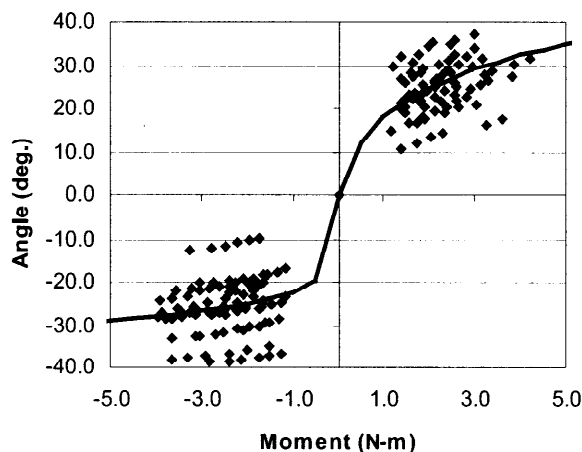


**Figure 1:** A plot of all the static flexion and extension flexibility data for 15 female O-C2 motion segments. Also shown is the logarithmic fit of the data. Separate functions are used for flexion and extension.

The results for all the O-C2 motion segments are shown in Figure 1. In order to find a functional relationship between moment and angle, the data were averaged at each load step, and then fit with a nonlinear function of the form:

$$\theta = A0 \ln(A1 \cdot M + 1)$$

where  $\theta$  is the angle,  $M$  is the applied moment, and  $A_0$  and  $A_1$  are model constants. This function is used for all the curve-fits in this report because it has been widely used to model the non-linear behavior of soft tissues. Because the independent variable (moment) was not the same for all specimens (due to frictional losses in the system), individual flexibility functions were determined for each specimen using the above function. The results for the set of functions were then averaged at every 0.5 N-m and fit for a second time. The coefficients for the curve are given in Table 1.

**Table 1: Coefficients for the Logarithmic Model**

	<u>Flexion</u>		<u>Extension</u>	
	A0	A1	A0	A1
O-C2	11.94	3.502	4.096	226.1
O-C2*	17.81	0.850	7.551	7.959
C3-4	4.668	3.582	4.962	1.459
C3-4*	4.210	3.356	9.103	0.412
C5-6	3.787	10.22	4.887	1.623
C5-6*	4.629	5.425	10.39	0.205
C7-1	2.540	4.649	5.194	0.725
C7-1*	4.461	1.031	32.30	0.034

\* Coefficients for the fits of the dynamic failure data from 0 to 20 N-m

### **Tolerance for Upper Cervical Spine Bending Injury**

The segments used in the above bending tests were failed in either flexion or extension. The moments were applied using pneumatic pistons. The loading rate was the maximum that could be achieved using our 100 psi system. The rates were dependent on the stiffness of the specimen, and were on the order of 90 N-m/second (Figure 2).

The failures produced in these tests included Type III dens fractures, atlanto-occipital dislocations, and failures of the fixation. Bending tests produce large tensile stresses, which place great demands on the fixation. It is impossible to achieve good fixation without creating stress concentrations in the bone. Consequently, any osseous injuries that originate in, or propagate through, the fixation points occur at levels below the real tolerance. In addition, the stress raisers reduced the strength of the vertebrae, increasing the probability of a bony failure as opposed to a soft tissue failure.

The average moment at failure for the flexion tests was  $23.66 \pm 3.42$  N-m at an angle of  $56.23 \pm 2.80$  degrees (Table 2). The average moment at failure for the extension tests was  $43.30 \pm 9.26$  N-m at an angle of  $50.20 \pm$  degrees. The difference in strength was statistically significant ( $p < 0.01$ ). The angles at failure are not significantly different ( $p > 0.2$ ).

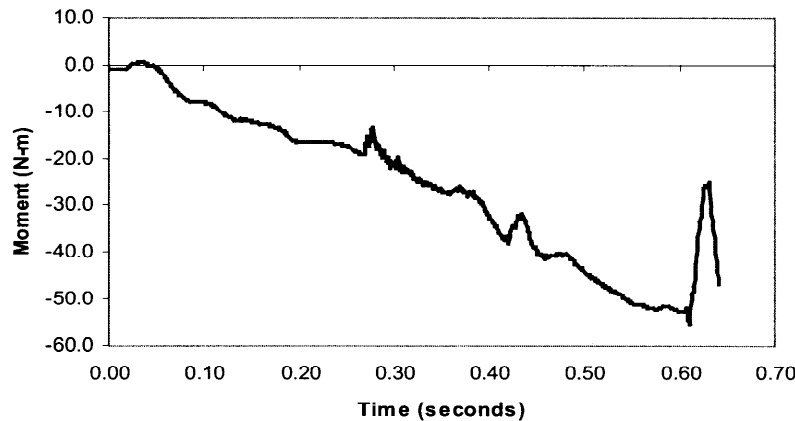


**Figure 2:** Moment history for an extension failure test. The failure occurs at a time of 0.62 seconds, and at a moment of 53 N-m.

All the failures were included in the statistical analyses of tolerance, including those that were judged to be due to stress concentration at the casting. Therefore, the moment values that are reported in Table 2 are a lower bound of tolerance in the female cadaver. Interestingly, the Type III dens fractures were produced in both flexion and extension. These fractures have been previously attributed to shear, compression, and extension. Realizing that moments must be supported, in part, by tensile loads in the anterior most portions of the cervical spine, we hypothesize that the C1-C2 injury mechanism in airbag deployments is the result of tensile stresses in the alar and apical ligaments due to combined tension and bending. The resulting tension and bending of the dens causes it to fracture at its base in C2.

**Table 2:** Failure Data for Upper Cervical Spine Motion Segments. *(Highlighted values were not included in the statistical analysis because: \*there was contact between the head or maxilla and the casting cup, which enables the reaction of large moments, \*\*the specimen had fused occipital condyles)*

ID	Flexion		ID	Extension	
	N-m	Angle		N-m	Angle
b03fo2*	68.62	56.99	I0995	45.19	na
b07fo2*	23.77	58.50	b04fo2	34.46	39.74
b09fo2	27.15	55.16	b05fo2	30.03	35.92
b10fo2*	45.91	62.25	b06fo2**	26.64	21.35
b14fo2	24.73	58.49	b11fo2*	65.52	54.36
b15fo2	19.00	52.75	b12fo2	36.86	59.18
			b13fo2	52.60	na
			b16fo2	42.76	na
			b17fo2	57.46	56.53
			b18fo2	47.05	59.63
Mean	23.66	56.23	Mean	43.30	50.20
Stdev	3.42	2.80	Stdev	9.26	11.43

### **Dynamic Flexibility of the Upper Cervical Spine**

Data from the 15 failure tests were analyzed to produce dynamic moment-angle relationships. The logarithmic model for the dynamic flexibility was derived using the same methodology as the static flexibility. However, the individual moment-angle plots for each motion segment were fit from 0 to  $\pm 20$  N-m. Data above 20 N-m was not used because that was the lowest moment value for which we had dynamic data for all the specimens. The O-C2 failure tests show that the motion segments are stiffer when loaded dynamically. Figure 3 illustrates the differences in the exponential fits for the static and dynamic data. The coefficients for the dynamic model are reported in Table 1.

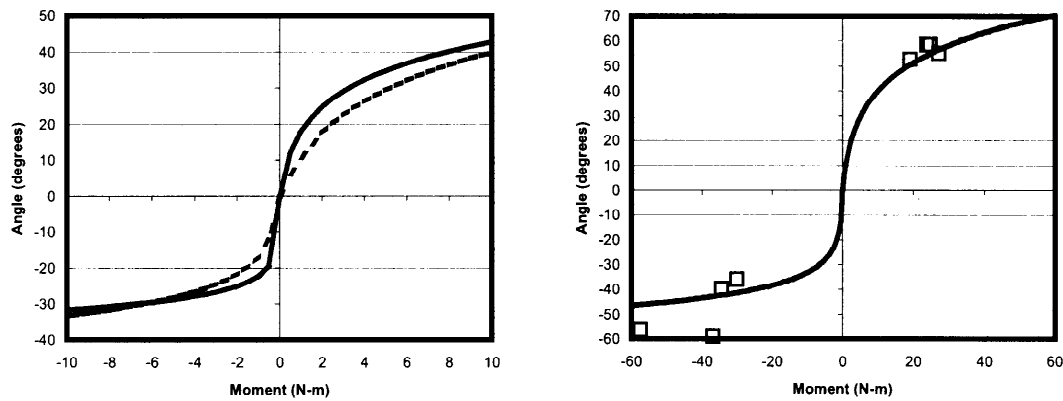


**Figure 3:** *Left:* Plots of the logarithmic fit of the O-C2 static flexibility data (solid line) and the dynamic failure data (dashed line). The static response is more flexible in both flexion and extension, illustrating the stiffening effect of increased loading rate. *Right:* A plot of the logarithmic fit of the dynamic O-C2 failure data, showing the flexion and extension failure points.

### **Static Flexibility of the Lower Cervical Spine**

The static flexibilities of lower cervical spine motion segments were determined using the same methodology (described above) as for the upper cervical spine motion segments. The lower cervical spine motion segments tested were C3-4, C5-6, and C7-T1. The coefficients for the logarithmic fits are shown in Table 1, and the curves are shown in Figure 4.

### **Tolerance for Lower Cervical Spine Bending Injury**

Failure testing was performed on the cervical spine motion segments using the same methodology (described above) as for the upper cervical spine motion segments. Multiple comparison testing of the moments at failure found significant differences between the some of the lower cervical spine motion segments and the O-C2 motion segments. The results of these tests are summarized in Table 3. All the moment data from the flexion and extension failure tests were grouped to determine average moments and angles at failure. For the flexion tests, the

moment tolerance is  $17.41 \pm 6.22$  N-m at an angle of  $19.33 \pm 5.39$  degrees. For the extension tests, the moment tolerance is  $21.22 \pm 7.61$  N-m at an angle of  $20.45 \pm 7.19$  degrees.

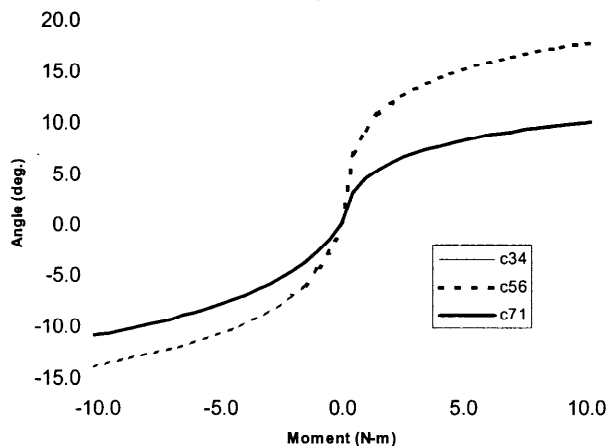


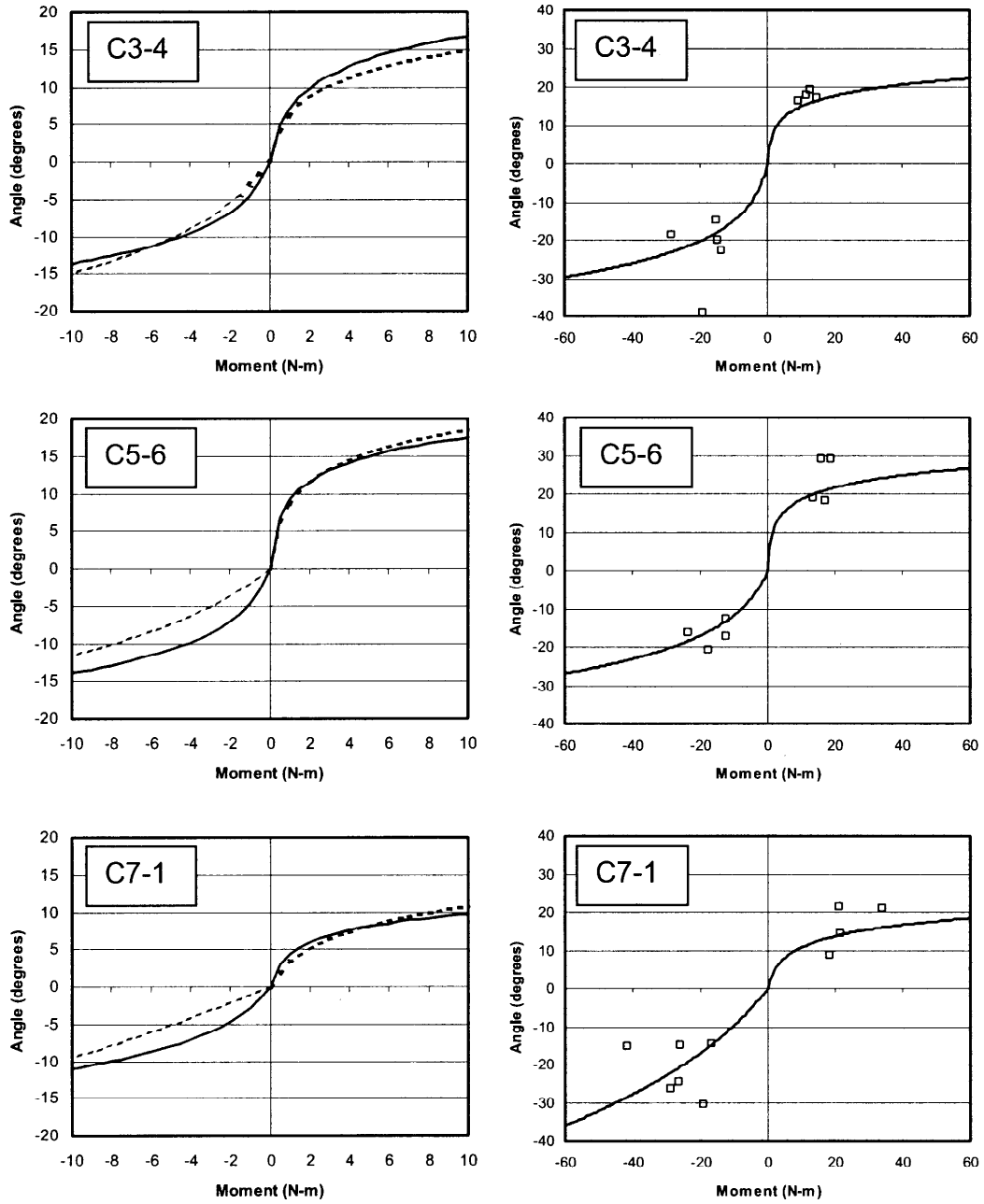
Figure 4: Plots of the static C3-4, C5-6, and C7-T1 logarithmic models.

Table 3: Summary of Differences in Motion Segment Tolerance (O means  $p < 0.05$ )

	Flexion				Extension			
	O-C2	C3-4	C5-6	C7-1	O-C2	C3-4	C5-6	C7-1
O-C2		X	X	X		O	O	O
C3-4	X		X	O	O		X	X
C5-6	X	X		X	O	X		X
C7-1	X	O	X		O	X	X	

**Dynamic Flexibility of the Lower Cervical Spine**

Dynamic flexibilities were determined for the lower cervical spine motion segments using the moments and angles measured in the failure tests. For the most part, the specimens failed between 10 and 20 N-m. Logarithmic fits of the individual failure tests were averaged up to 20 N-m and then fit a second time to produce log models for each motion segment. The static and dynamic models are shown in Figure 5. In general, the dynamic response is slightly stiffer than the static response.



**Figure 5:** *Left:* Plots of the logarithmic fit of the static flexibility data (solid line) and the dynamic failure data (dashed line). *Right:* A plot of the logarithmic fit of the dynamic failure data, showing the flexion and extension failure points.

## Design Parameters for Tensile Responses

We are in the early stages of a multiyear program to fully characterize the tensile responses of the ligamentous human cervical spine. To date, we have performed tests on five specimens out of an estimated 80. The data presented in this section is preliminary and will change as the program progresses.

### Tensile Stiffness of the Whole Ligamentous Cervical Spine

Tension tests have been conducted on five cervical spines from male cadavers. The test battery includes preconditioning, end-condition testing, and viscoelastic testing. These were performed on whole head/cervical spine preparations. Non-destructive testing was conducted to determine the quasi-static tensile stiffness of the whole neck. Displacements were applied at a rate of 2 mm/sec to a peak load of 300 Newtons. This testing was conducted with the head and the first thoracic vertebra (T1) fully constrained (a fixed-fixed end condition). Results for the five specimens are shown in Figure 6.

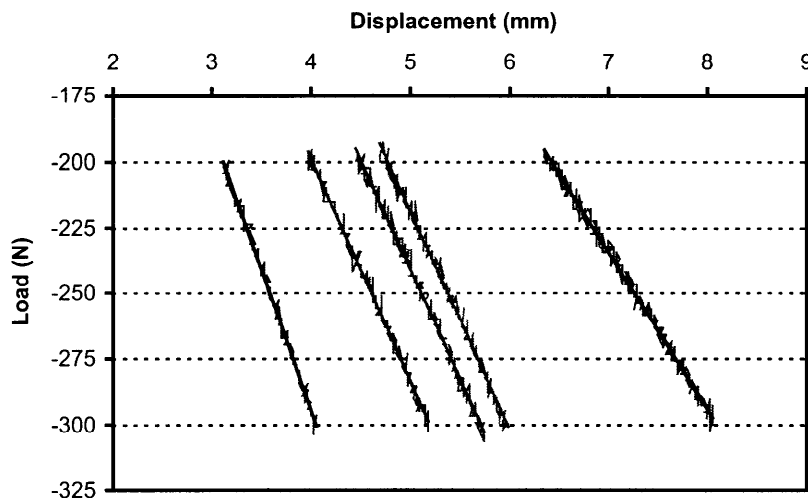


**Figure 6:** Tensile stiffness curves for five human head/neck preparations tested in a fixed-fixed end condition. The response is nonlinear; therefore, only the data between  $-200$  and  $-300$  Newtons was regressed. The stiffnesses and correlation coefficients are: a)  $106.9$  N/mm ( $0.9908$ ) b)  $85.06$  N/mm ( $0.9924$ ) c)  $83.44$  N/mm ( $0.9927$ ) d)  $83.09$  N/mm ( $0.9908$ ) e)  $59.74$  N/mm ( $0.9937$ ).

### **Tensile Tolerance Data for Motion Segments**

The failure testing was conducted on motion segments rather than whole cervical spines. This was done because a pilot study showed that it was very difficult to produce clinically observed failures at points other than the level of the casting. Therefore, the cervical spines were sectioned after the above series of nondestructive tests, recast, and loaded to failure. The motion segments tested were O-C2, C4-5, and C6-7.

Prior to the failure tests, a battery of nondestructive tests were run to determine viscoelastic properties and force deflection properties. The specimens were failed at a rate of two mm/sec in a fix-free end condition. The tolerances of the motion segments are summarized in Table 4.

**Table 4:** Tensile Tolerance of Motion Segments

	<i>C6-7</i>	<i>C4-5</i>	<i>O-C2</i>
<i>ID #</i>	<i>N</i>	<i>N</i>	<i>N</i>
07	1660		2519
08	2077	1691	2148
09	1769	1509	2310
10	1861	1939	2092
11	1837	2021	2820
<i>Ave</i>	1841	1790	2378
<i>St Dev</i>	153	234	298

Multiple comparison testing was done to find differences between the tensile tolerances of the motion segments. A Tukey test level found that the O-C2 motion segment is significantly stronger than both the lower motion segments at the 0.05 significance level. The same test revealed no significant difference between C4-5 and C6-7.

### **Tensile Stiffness of Cervical Spine Motion Segments**

The stiffness properties of the motion segments were tested in with fixed-fixed end conditions. Prior to testing, the specimens were mechanically stabilized with 30 cycles of load varying from 0 to approximately 150 Newtons. The specimens were then loaded to 300 Newtons of tension at a rate of 2 mm/s. The resulting force-displacement curves were fit with a quadratic and then averaged from 0 to 325 Newtons. The results are shown in Figure 7.

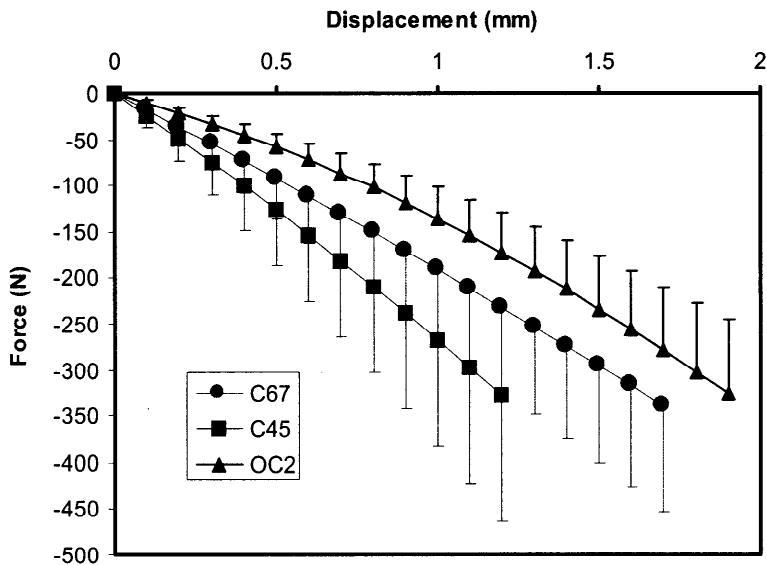


**Figure 7:** Tensile responses of the O-C2, C4-5, and C6-7 motion segments. The O-C2 segment is the most compliant.

## The Effects of the Musculature

The tolerance data for bending and tension shows that the ligamentous upper cervical spine is stronger than the ligamentous lower cervical spine. However, this is not consistent with the epidemiology tensile neck injury. Although it is expected that the weakest point would be the site of failure, the Special Crash Investigation documents a large number of upper cervical spine injuries in both adults and children. This discrepancy is most likely due to the effects of the musculature. The muscles of the cervical spine share tensile loads with the ligamentous cervical spine by providing a parallel load path. Such load sharing increases the overall strength and stability of the neck, and provides greater protection to the caudal motion segments because of the larger size and number of muscles in the lower cervical spine. Cadaveric studies, which include a small contribution from passive neck muscles (postmortem muscle is less stiff than live passive muscle) also support these results. Finally, the autopsy results in the SCI report disruption of the upper cervical spine musculature near the injury sites; a clear sign that the muscles are carrying load during these injury events.

Understanding the contribution of the neck muscles is the subject of ongoing research. Using a typical 50th percentile male volunteer combined with cadaver dissection, the total neck muscle physiologic cross sectional area has been found to be approximately 52.6 cm<sup>2</sup>. In this study, we have captured approximately 95% of the total muscle area in the neck. Therefore, the total muscle area is closer to 55.4 cm<sup>2</sup>. Isometric tetanic muscle stresses in the published literature vary widely, with values typically between 0.2 MPa and 1.0 MPa. Isometric stress in mammalian skeletal muscle based on true cross-sectional area during high strain rate loading measured in our lab was 0.44 MPa. Converting this to isometric stress based on physiologic cross sectional area gives a value of 0.327 MPa. Elongation of muscles which are active (an eccentric contraction) increases the stress in the muscle. Increases in the isometric value by a factor of 1.5 are commonly used. Our experience shows that at large strains (on the order of

45%) the stress has increased by a factor of two. Since the strains at tensile neck injury are likely smaller, using a value of 1.5 seems appropriate. Therefore, an estimate of the total tensile force that can be generated by stimulated neck muscles is:  $(55.4E-4 \text{ m}^2) \times (0.327E6 \text{ MPa}) \times 1.5 = 2582$  Newtons. This does not include the contributions of the passive muscles, which can be large at large strain.

Current understanding of the role of muscle during neck injury is confounded by factors including muscle recruitment and pre-impact awareness. Obviously, not all muscles will be recruited and not all muscles will work to oppose the tensile displacement, particularly in the presence of head extension rotation. At this time, there are no data on the proportion of muscles engaged in load sharing with the ligamentous cervical spine during impact loading. We are currently engaged in modeling efforts that will answer some of these questions. Meanwhile, we can calculate some crude estimates for muscle force by making certain assumptions. If we neglect the contribution of passive tissues and assume that 70% percent of the available muscle force is engaged in load sharing, then the total force generated is 1800 Newtons. Since the tensile tolerance of the ligamentous C4-5 motion segment is also approximately 1800 Newtons it seems reasonable to use two times this value as the tolerance of the muscular neck. Hence, our support for the value of 3600 Newtons as a tensile human tolerance.

Because of the differences in stiffness between the ATD neck and the human neck, a tolerance larger than 3600 may be appropriate as an ATD injury reference value. Our numerical study entitled "Effects of Upper Neck Joint Stiffness on Measured Moments in the Hybrid III Dummy During Airbag Loading" provides some insight into the effects of stiffness on peak neck loads. That study showed that tensile loads increase when the axial neck stiffness is changed from cadaver values to Hybrid III dummy values. The resultant neck load increased 25% from 4394 Newtons to 5502 Newtons. The tensile component of load increased 35% from 3505 Newtons to 4744 Newtons. These ratios justify the use of ATD injury reference values in the range of 4500 to 4860 Newtons.

## **Facilities for Neckform Testing**

The Duke University Biomechanics Laboratory has several facilities for the testing of neckform prototypes. Apparatuses are available to assess design and performance in bending, compression, and tension (described below). Design iteration testing will produce criteria on which to modify the neckform based on comparing the results of the design tests with the design criteria. Performance tests measure biofidelity by statistical correlation of the measured variables with the performance criteria.

### **Bending Design Test:**

Flexion and extension flexural rigidity of the neckforms will be measured and compared to the Hybrid III neckform flexural rigidity using the pure moment test frame. Two 100 psi pneumatic cylinders will apply up to 60 N-m quasi-statically using a series of cables and pulleys. Deformation will be measured using biplanar CCD cameras and stereophotogrammetry. Neckform flexural rigidity will be compared with the Hybrid III flexural rigidity.

### **Bending Performance Test**

The Part 572.33 pendulum test will be implemented to test dynamic bending performance (Backaitis, 1994). Briefly, a 1.867 m structural steel pendulum will impact an aluminum honeycomb (Hexcel) such that neither the headform nor the neckform impact any other object. A pendulum accelerometer, an impact foam load cell and an occipital condyle three axis load cell will be used. The neckforms will be mounted to the pendulum using the Hybrid III neck adjusting bracket assembly (PNs78051-307 and 78051-303). A 1000 Hz CCD imager will be used to image video targets on the headform and neckform to determine head rotation. The results will be compared to the Mertz bending corridors.

### **Compression Design Test**

Neckforms will be tested in accordance with Pintar (1995) and compared to their head-neck compression corridors. Briefly, the prototype neckform-Hybrid III headform will be mounted to a Denton six-axis load cell and coupled to the upper platen of an MTS linear actuator. The neckform will be preflexed 20 degrees using a weight pulley apparatus described by Pintar. The actuator impact surface will be covered with 20 mm thick ensolite padding and will apply a 30 mm axial displacement at 4.0 m/s. An LVDT will quantify actuator displacement. All data will be acquired digitally and force-displacement data will be derived and compared with the compression design corridor.

### **Compression Performance Test**

The neckforms will be performance tested using our instrumented impact drop track. Padded (polyurethane foam) and unpadded impacts will be conducted with -15, 0, +15 degrees impact surfaces and the force-time histories of the headform and neckform will be compared with the compression performance corridors. In addition, the dynamic impact stiffness of the neckform will be calculated and compared with the design standard.

### **Tension Testing**

Tension testing will be performed in our cadaver tension frame. This frame is designed to apply tensile loads to head and neck forms at a variety of load points, and for a variety of end conditions. The force-time histories and the force-displacement characteristics will be compared with tensile performance corridors similar to the ones contained in this report.

## **Conclusions**

These data provide a preliminary basis for tolerance assessment and some design criteria for the next generation neckform. They also illustrate the far-field research necessary to more fully understand tension and bending cranio-cervical injuries. The currently active NHTSA programs will eventually fully characterize the tensile responses and the tolerances of the muscular human neck.